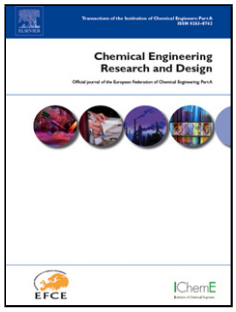

Title: Hybrid Simulation-Equation Based Synthesis of Chemical Processes

Authors: Natalia Quirante, Juan Javaloyes-Antón, José A. Caballero

PII: S0263-8762(18)30097-2
DOI: https://doi.org/10.1016/j.cherd.2018.02.032
Reference: CHERD 3061

To appear in:

Received date: 18-5-2017
Revised date: 23-9-2017
Accepted date: 20-2-2018

Please cite this article as: Quirante, Natalia, Javaloyes-Antón, Juan, Caballero, José A., Hybrid Simulation-Equation Based Synthesis of Chemical Processes.Chemical Engineering Research and Design https://doi.org/10.1016/j.cherd.2018.02.032

Hybrid Simulation-Equation Based Synthesis of Chemical Processes

Natalia Quirante, Juan Javaloyes-Antón, and José A. Caballero*.

Institute of Chemical Processes Engineering. University of Alicante, PO 99, E-03080 Alicante, Spain.

*Corresponding author: *Tel*: +34 965902322. *Fax*: +34 965903826. *E-mail address*: caballer@ua.es

Graphical abstract

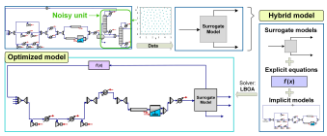

Highlights

- A methodology for the optimization of complex chemical processes is developed.
- A hybrid model is solved (simulation units, Kriging models and explicit equations).
- Optimization of VCM process is performed to show the performance of our approach.
- This approach has proved to be robust and reliable to solve complex problems.
- Additionally, heat integration and economic feasibility are studied.

Abstract

A challenging problem in the synthesis and design of chemical processes consists of dealing with hybrid models involving process simulators and explicit constraints. Some unit operations in modular process simulators are slightly noisy or require large CPU times to converge. In this work, this problem is addressed by combining process simulators and surrogate models. We have replaced some unit

operations, which cannot be used directly with a gradient-based optimization, by surrogate models based on Kriging interpolation. To increase the robustness of the resulting optimization model, we perform a degree of freedom analysis and aggregate (or disaggregate) parts of the model to reduce the number of independent variables of the Kriging surrogate models (KSMs). Thus, the final model is composed of KSMs, unit operations (maintained in the process simulator) and also explicit equations.

The optimization of the well-known vinyl chloride monomer (VCM) production process is performed to test the proposed approach. The effect of the heat integration is also studied. In addition, the economic feasibility of the optimized process is calculated assuming uncertainty in raw material and product prices.

Keywords: simulation, optimization, MINLP, Kriging algorithm, Vinyl Chloride Monomer process.

1. Introduction

Methodologies for the synthesis of chemical processes can be classified into two different categories: sequential-conceptual methods and superstructure optimization-based methods.

Sequential methods follow a natural hierarchy between the engineering decisions to obtain a chemical process flowsheet (Douglas, 1985, 1988). This approach is commonly used because the original problem is divided into a set of sub-problems that reduce the complexity of the initial problem. However, due to its sequential nature, this approach cannot guarantee an optimal solution since it ignores the different trade-offs between the various objectives of the prior stages.

Superstructure optimization-based methods consider the complete network which is composed of all the unit operations, their connections, and other constraints (Grossmann, 1985; Yeomans and Grossmann, 1999). The solution of the mathematical model specifies which of the initial units and connections are kept in the optimal structure. These methods are used because they offer a simultaneous optimization of the process structure and the operating conditions. However, superstructure optimization-based methods are complex to solve due to the resulting models, usually large-scale non-convex mixed-integer nonlinear programs (MINLP). The general algebraic form of these MINLP optimization problems is shown in Eq.(1).

$$\begin{aligned} &\min_{x,y} f(x,y) \\ &s.t.\ h(x,y) = 0 \\ &\quad g(x,y) \le 0 \\ &\quad x \in \mathbb{R}^n, \qquad y \in \{0,1\}^t \end{aligned} \tag{1}$$

where *f(x,y)* is the objective function (e.g., economic, environmental, etc.); *h(x,y)* are the equations that describe the behavior of the system (e.g., mass and energy balances, reaction rates, etc.); and *g(x,y)* are inequality constraints that define process specifications (e.g., product purities, maximum temperature allowed, etc.). The real n-vector *x* represents the continuous independent variables, and the t-vector *y* represents the discrete independent variables.

When a sequential-modular process simulator is used as a black box to compute the objective function and/or the equations that describe the behavior of the system (equality constraints in the previous MINLP problem), different approaches can be employed to solve the resulting optimization problem. We can try to address the problem directly by using commercial derivative-based solvers (e.g., DICOPT, ALPHAECP, SBB…) or metaheuristic algorithms (e.g., genetic algorithms or particle swarm optimization algorithms). However, some important drawbacks arise with both paths.

On the one hand, when mathematical programming solvers are used, the following challenges arise. First, due to the nonlinearities and non-convexities inherent to some unit operations and thermodynamic models, these methods do not guarantee a global solution and can be easily stuck in local solutions. Moreover, the solution depends very sensitively on initial values. However, what is much more important is the fact that the objective function and/or the set of constraints are analytically intractable (discontinuous, non-differentiable, and inherently noisy). Hence, derivatives of the objective and/or constraint functions with respect to the independent variables must be calculated by numerical differentiation (which limits the accuracy and effectiveness of such solvers).

Derivatives calculated by perturbation can be very expensive to compute, and even in the case in which the CPU time is not excessive, some unit operations introduce numerical noise. Thus, an accurate derivative cannot be obtained. Of course, all these models are perfectly valid for simulation purposes, but even relatively small differences in two instances –completely negligible in any simulation– prevent the calculation of accurate derivatives (a detailed discussion can be found in Caballero and Grossmann (2008)).

On the other hand, metaheuristic techniques (which belong to a class of optimization strategies that does not require gradient information, i.e., derivative-free optimization (DFO) methods) seem to be well suited to simulation-based optimization when sequential-modular simulators are used. This is because they only require the values of the objective function. Of course, there are significant disadvantages of not having derivative information. We cannot expect that the performance of DFO methods matches those of derivative-based methods. In particular, the scale of the problems that can be efficiently solved by DFO algorithms does not exceed a few tens of variables (Conn et al., 2009). Besides, these techniques are not able to guarantee the optimality of the solution found, although they are designed to have the ability to escape from local optima. In addition, DFO algorithms normally require a large number of function evaluations, and perhaps, one of the most important disadvantages is that DFO algorithms exhibit poor performance in highly constrained systems. Generally, these algorithms handle the constraints by adding a penalty to the objective function to account for infeasibility.

An added difficulty regardless the optimization technique is related to the convergence of flowsheets with several recycle streams. As simulations become more complex, the robustness (in terms of convergence) decreases and the simulator becomes prone to errors.

These approaches for solving synthesis problems are not new. A considerable amount of literature supports the synergy achieved through the smart integration of chemical process simulators with an external optimizer based on gradient information (Balas, 1979; Brunet et al., 2012; Caballero et al., 2005; Díaz and Bandoni, 1996; Diwekar et al., 1992; Navarro-Amorós et al., 2014; Raman and Grossmann, 1994; Reneaume et al., 1995) and metaheuristic techniques (Aspelund et al., 2010; Bravo-Bravo et al., 2010; Chen et al., 2014; Dantus and High, 1999; Eslick and Miller, 2011; Gross and Roosen, 1998; Gutiérrez-Antonio and Briones-Ramírez, 2009; Javaloyes-Antón et al., 2013; Leboreiro and Acevedo, 2004; Odjo et al., 2011; Vazquez–Castillo et al., 2009).

Some researchers have proposed frameworks to reduce the complexity of the optimization models through the use of surrogate models (Jones et al., 1998; Shao et al., 2007; Won and Ray, 2005; Xiong et al., 2007). A surrogate model is a set of mathematical functions, based on data generated from the simulation. In this way, the optimization of an analytically tractable and computationally cheap surrogate model replaces the original black box process. Most often, for complex systems, it is

recommended to disaggregate the whole process into smaller units and model each block separately, ensuring that all relevant connectivity variables have also been included (i.e., component flows, temperatures, and pressures of each stream).

The main novelties of the proposed approach are at the modeling stage and at solution stage.

At the modeling level, as far as we know, the deterministic optimization of problems related to large-scale superstructures with a non-fixed topology dealing with hybrid models involving process simulators, explicit constraints and surrogate models for dealing with noise units and third-party modules (i.e., non-numerical noisy proprietary models) has never been studied.

At the solution stage, we use a logic-based algorithm -the Logic-Based Outer Approximation algorithm (Turkay and Grossmann, 1996)-. Logic-Based Algorithms do not require the reformulation of the problem as an MINLP. The NLP sub-problems can, therefore, be efficiently solved. The numerical efficiency of the optimization is improved by using a distributed approach for surrogate models (we use small surrogate models with a reduced number of degrees of freedom instead of a single large model). The advantage is that we minimize the necessity of resampling during the optimization (Biegler et al., 2014; Quirante et al., 2015).

In this work, we have used the Kriging algorithm to build the surrogate models since they are computationally efficient and they need relatively small sampling data to be built. Several works have been carried out to overcome the challenges of simulation-based optimization using surrogate models based on Kriging interpolation. Caballero and Grossmann (2008) studied the optimization of a disaggregated flowsheet using Kriging models, obtaining unit operations with low-level noise. Henao and Maravelias (2011) used artificial neural networks for disaggregating models. Other works have modeled and optimized chemical processes using Kriging-based techniques (Davis and Ierapetritou, 2007; Palmer and Realff, 2002a, b; Quirante and Caballero, 2016; Quirante et al., 2015). A review of Kriging applications in simulation was made by Kleijnen (2009).

The objective of this work is to develop an optimization-based simulation tool that uses a process simulator as calculation engine, where surrogate models based on Kriging interpolation replace those unit operations that introduce numerical noise or need a large CPU time to converge. At the same time, it allows us to introduce explicit equations in such a way that the resulting model includes surrogate

models, unit operations maintained in the process simulator and explicit equations. The rest of this article is organized as follows. In the next section, we discuss the main features of the proposed approach. Then, to illustrate this approach, we use the superstructure proposed by Turkay and Grossmann (1998) for the synthesis of the vinyl chloride monomer (VCM). To complete the study of the VCM process, the influence of the heat integration on the profit of the process is studied. Besides, the economic feasibility of the optimized VCM process is evaluated assuming uncertainty in raw material and product prices. Finally, the conclusions of this work are summarized at the end of the paper.

2. Methodology

In the proposed approach, simulation-based optimization of complex processes is performed using derivative-based solvers. The superstructure, which includes all the alternatives of interest of the process that we need to optimize, is implemented at the level of the process simulator, with the added feature that those unit operations that are inherently noisy and/or expensive to converge (in terms of CPU time) are replaced by surrogate models based on Kriging interpolation (e.g., distillation columns and reactors). The units that do not introduce numerical noise (such as mixers, splitters, coolers/heaters, compressors, valves or pumps) are maintained in the process simulator. The surrogate models are built in MATLAB from training data sets obtained from the process simulator. In addition, the equations related to capital and operating costs are implemented as explicit equations.

As discrete decisions have to be made in order to select the different paths considered in the superstructure, the mathematical model of the optimization problem follows the generalized disjunctive programming (GDP) framework (Balas, 1979; Raman and Grossmann, 1994). Then, the disjunctions that represent the discrete decisions and involve models in the process simulator, are systematically converted to algebraic equations by means of the Big-M formulation (Nemhauser and Wolsey, 1988). Those discrete decisions, in terms of explicit equations, are either reformulated using a Big-M or a hull reformulation, depending on the characteristics of the equations. In general, convex constraints –that include all linear constraints– are reformulated using a convex hull approach and the rest by the Big-M formulation. The logic propositions are reformulated to a set of linear algebraic constraints (see for example Grossmann and Trespalacios (2013)).

The methodology followed to develop the simulation-based optimization of complex process superstructures can be divided into the following main steps. The first step is the simulation stage. The objective is to build our superstructure in a chemical process simulator. We can use process simulators such as Aspen Plus or Aspen HYSYS and take advantage of that they are developed following an objected-oriented approach. This architecture makes it possible to transfer functionalities to other software applications (Aspen Technology, 1994-2015). Thus, Aspen HYSYS (or Aspen Plus) can be accessed from external programs (such as MATLAB or Python) via Automation. This is a key feature since we will be able to develop an executive program to automate the surrogate model building step and to interface the final model, which is formed by unit operations implemented in the process simulator, surrogate models, and explicit equations, with the derivative-based optimization solver.

After simulating our chemical process superstructure, we identify the unit operations or set of unit operations that introduce numerical noise and/or are expensive to converge. These units or blocks of units are replaced by surrogate models.

In this work, we focus on the Kriging interpolation (Krige, 1951) to build the surrogate models. Kriging was developed by Daniel G. Krige during his Master's degree (Krige, 1951).

This fitting is composed of a polynomial expression, $f(x)$, and a term corresponding to the deviation of that polynomial, $Z(x)$.

$$y(x) = f(x) + Z(x) \tag{2}$$

The spatial correlation function $R(x_i,x_j)$ can fit a scale factor σ^2 to the data, given the covariance for two points x_i and x_j. The extended exponential alternative for the spatial correlation function in Kriging models was used by Sacks et al. (1989).

$$R\left(x_i, x_j\right) = \exp\left(-\sum_{l=1}^{d} \theta_l \left(x_{i,l}, x_{j,l}\right)^{P_l}\right) = \prod_{l=1}^{d} \exp\left(-\theta_l \left(x_{i,l}, x_{j,l}\right)^{P_l}\right) \tag{3}$$

where θ_l ($\theta_l \geq 0$) shows how fast the correlation goes to zero, and P_l ($0 \leq P_l \leq 2$) is the smoothness of the function, usually a Gaussian Kriging ($P_l = 2$).

A thorough description of the Kriging interpolation method can be found in the literature (Jones, 2001; Jones et al., 1998; Quirante et al., 2015).

In order to build robust and accurate surrogate models, an efficient distribution of the training points becomes mandatory. For this purpose, an a priori infill procedure, the 'maxmin' approach, has been used. This method maximizes the minimum distance between two training points (a broad description of the 'maxmin' approach can be found in Quirante and Caballero (2016)). First, we assign 2^D points to the D-dimensional vertices of the hypercube that constitutes the feasible search space. Then, the remaining $N-2^D$ points are uniformly distributed following the 'maxmin' approach. Thus, we ensure that the complete domain is contained in the convex hull formed by all the sampling points and we are not doing 'extrapolations' in any moment.

One of the major drawbacks of using surrogate models is that the surrogate model could not reproduce the original model with enough accuracy. Even in the case where we can ensure a good numerical conditioning (for example, small errors in the surrogate model do not reproduce a snowball effect and propagate throughout the entire optimization model), the lack of accuracy in the surrogate model could eventually end with a non-realistic result. To overcome that problem, some researchers have proposed different strategies based on using <<trust regions>> (Biegler et al., 2014; Caballero and Grossmann, 2008; Quirante et al., 2015). The main idea is to perform an initial sampling and then contract, expand or move the region by resampling when needed. Finally, the surrogate model in the final point must be able to reproduce the actual model –some implementations also require an accurate reproduction of the gradient–. Alternatively, if the number of degrees of freedom of a model is small enough (up to 5 degrees of freedom), it is possible to initially perform an exhaustive sampling that allows us to generate a surrogate model accurate enough to avoid resampling. Of course, this second approach is not always possible. In any case, we have to deal with the tradeoff between the number of initial points and the number of major iterations. A large number of sampling points could require large CPU times in sampling, model calibration, and Kriging interpolation, but the number of resamples to recalibrate the surrogate model in different regions should be lower.

Even though reducing the degrees of freedom to develop surrogate models that do not require recalibrations is not always possible, sometimes we can aggregate (or disaggregate) some models (unit operations in a modular simulator) and reduce the number of independent variables without losing accuracy. In this work, we have followed this approach.

Next, we have followed a disaggregated approach to developing the system, which has the following characteristics:

- All the unit operations were simulated using Aspen HYSYS v.8.4 (Aspen Technology, 1994-2015).
- The calibration of the Kriging surrogate models was done using MATLAB (The Mathworks, 2014).
- The model, objective function, constraints, and surrogate models were implemented using an in-house algorithm (Caballero et al., 2014) of the basic Branch and Bound method interfaced with TOMLAB-MATLAB (Holmström, 1999).
- We have connected MATLAB with Aspen HYSYS to optimize the process.

The application of the proposed methodology is illustrated with the optimization of the benchmark process to produce Vinyl Chloride Monomer (VCM), following the superstructure proposed by Turkay and Grossmann (1998). The selection of this case study is basically due to the large amount of information and data that can be found in the literature. It has been studied by different researchers with different approaches and, therefore, it is easy to reproduce.

We have considered this case study because it contains the complexity suited to test the proposed methodology:

- A non-fixed topology with a large number of equipment (55 process units including compressors, heat exchangers, pumps, separators, different types of reactors, and different sets of conventional and thermally coupled distillation columns) that give rise to a large number of possible alternatives.
- Reactors and distillation columns, which are slightly noisy and/or difficult to converge and, therefore, can be replaced by surrogate models.
- Unit operations that do not introduce numerical noise (like mixers, splitters, compressors, heat exchangers and pumps) and can be maintained in the process simulator.
- Recycle blocks, which are transformed to explicit equations avoiding inefficient and time-consuming iterations.
- Third-party modules developed in Matlab to calculate sizes and costs.

3. Case study: Vinyl chloride monomer production process

Vinyl chloride monomer (VCM) is one of the world's most important and largest commodity chemicals (Modler et al., 2015). It is used mainly for the production of polyvinyl chloride (PVC), which is the third-most widely produced synthetic plastic polymer (Fischer et al., 2014).

In the past, vinyl chloride was first produced by treating 1,2-dichloroethane with a solution of potassium hydroxide in ethanol. One of the initially patented processes to produce vinyl chloride implicated reacting acetylene and hydrogen chloride using mercuric chloride as a catalyst. This method was widely used during the 1930s and 1940s, but nowadays, VCM is produced by pyrolytic decomposition of ethylene dichloride (EDC). EDC is produced by the direct chlorination of ethylene and by the oxychlorination of ethylene in the presence of hydrogen chloride and oxygen. Vinyl chloride is produced by the pyrolysis of EDC, obtaining hydrogen chloride as a co-product, which is recycled and completely used in the oxychlorination of ethylene.

There are several combinations of technologies for vinyl chloride production. In Figure 1, the superstructure considered is shown. The VCM superstructure considered in this paper is based on the process given by Turkay and Grossmann (1998) and consists of three sections: direct chlorination, oxychlorination, and pyrolysis.

The main reactions involved in the process are:

Direct chlorination: $C_2H_4 + Cl_2 \rightarrow C_2H_4Cl_2$

Oxychlorination: $C_2H_4 + 2HCl + 0.5O_2 \rightarrow C_2H_4Cl_2 + H_2O$

Pyrolysis: $2C_2H_4Cl_2 \rightarrow 2C_2H_3Cl + 2HCl$

Some considerations, which are described below, have been taken into account in order to reduce the number of independent variables during the building of the Kriging metamodels.

3.1. Objective function

The objective is to determine the best flowsheet topology to maximize the profit of the plant.

The objective function includes raw material costs, costs associated with utility consumptions (electricity, cooling water, refrigerant, steam, and fuel oil), annualized investment costs for equipment, and income from the sales of vinyl chloride and trichloroethane (TCE) by-product. The estimation of the capital costs is calculated using the correlations given by Turton et al. (2013). The objective function is determined by the following expression:

$$profit = \sum_{p} MF_p \cdot price_p - \left(\sum_{r} MF_r \cdot price_r + C_{op} + F \cdot C_{cap} \right) \quad (4)$$

where MF_p is the mass flow of the products sold, $price_p$ is the price of the products sold, MF_r is the mass flow of the raw materials bought, $price_r$ is the price of the raw materials bought, C_{op} is the operating cost per year, F is the annualization factor, and C_{cap} is the capital cost of the equipment. Prices and costs have been updated by the global CEPCI cost index of 2015. The annualization factor is calculated by the equation recommended by Smith (2005) where we have considered a fixed interest rate of 10 % and a horizon time of 8 years.

The prices of the products, raw materials, and utilities are given in Table 1 (ICIS, 2015).

The superstructure presented in Figure 1 includes the alternatives explained below.

3.2. Direct chlorination

In the direct chlorination section (Figure 2), ethylene is chlorinated to EDC. The direct chlorination reactor operates at 55 – 100 ºC and 101.3 – 506.6 kPa. The conversion for the direct chlorination reaction under these conditions is 100 % and the selectivity to ethylene dichloride is greater than 99 % (McPherson et al., 1979). The exothermic reaction is catalyzed by ferric chloride catalyst. We modeled the direct chlorination reaction using kinetics derived from Wachi and Morikawa (1986) presented in appendix A.

3.2.1. Feed compression for direct chlorination system

The feed enters the process at low pressure (101.3 kPa) and must be compressed to a higher pressure where the reaction is feasible. For compression, we use a single compressor (single-stage compression) (K-100).

3.2.2. Heating/cooling before the direct chlorination reactor

The operating conditions selected in the reactor implies that the temperature of its inlet should be between 55 and 100 ºC. To get this, the resulting stream from the compressed feed has to be heated or cooled.

To model this situation, we define the Boolean variables Y_1 and Y_2 to select a heater or a cooler, respectively.

$$\begin{bmatrix} Y_1 \\ 55^{o}C \le T^{FeedDC,out} \le 100^{o}C \\ T^{FeedDC,in} \le T^{FeedDC,out} \end{bmatrix} \vee \begin{bmatrix} Y_2 \\ 55^{o}C \le T^{FeedDC,out} \le 100^{o}C \\ T^{FeedDC,in} \ge T^{FeedDC,out} \end{bmatrix} \quad (5)$$

where $T^{FeedDC,in}$ and $T^{FeedDC,out}$ are the temperatures entering and leaving the exchanger, respectively.

To simulate the heater (E-100), we use a heat exchanger using low-pressure steam as a hot utility. To simulate the cooler (E-101), we use a water-cooled heat exchanger using water as a refrigerant.

3.2.3. Reactor for direct chlorination

We have supposed that the reaction can take place in a CSTR in the presence of EDC liquid or without the presence of EDC, or in a PFR. To model the reactor alternatives, we define the Boolean variables Y_3, Y_4, and Y_5 to operate with a CSTR with addition of EDC (R-100), with a CSTR (R-101), or with a PFR (R-102), respectively.

$$\begin{bmatrix} Y_3 \\ 55^{o}C \le T^{CSTR\_EDC,DC} \le 100^{o}C \\ 101.3kPa \le P^{CSTR\_EDC,DC} \le 505.6kPa \\ 0.01kg/h \le F^{CSTR\_EDC,DC} \le 5kg/h \end{bmatrix} \vee \begin{bmatrix} Y_4 \\ 55^{o}C \le T^{CSTR,DC} \le 100^{o}C \\ 101.3kPa \le P^{CSTR,DC} \le 505.6kPa \end{bmatrix} \vee \begin{bmatrix} Y_5 \\ 55^{o}C \le T^{PFR,DC} \le 100^{o}C \\ 101.3kPa \le P^{PFR,DC} \le 505.6kPa \end{bmatrix} \quad (6)$$

where $T^{CSTR\_EDC,DC}$ is the temperature of the CSTR with addition of EDC, $P^{CSTR\_EDC,DC}$ is the pressure of the same reactor and $F^{CSTR\_EDC,DC}$ is the mass flow of EDC added to the reactor; $T^{CSTR,DC}$ is the temperature of the CSTR, $P^{CSTR,DC}$ is the pressure of the same reactor, $T^{PFR,DC}$ is the temperature of the PFR, $P^{PFR,DC}$ is the pressure of the PFR. The reactors are cooled using water as a refrigerant.

3.2.4. Cooling after the direct chlorination reactor

The stream leaving the direct chlorination reactor is considered to be cooled to 40 ºC in a water-cooled heat exchanger (E-102) using water as a refrigerant.

3.2.5. Separation system

The next step in the process is the separation system. The stream leaving the cooler (E-102) contains EDC produced, and unreacted ethylene and Cl_2. A distillation column (T-100) is used to remove the light components and obtain EDC with the desired composition. The distillation column operates at 101.3 kPa. A sensitivity analysis showed that the number of distillation trays and tray position did not have an important impact on the final results, so we fixed 10 trays with the feed in the 5th tray.

3.3. Oxychlorination

In the oxychlorination section (Figure 3), ethylene reacts with hydrogen chloride in the presence of oxygen. The reaction conditions are given as 180 – 225 ºC and 152.0 – 1621.2 kPa. The conversion under these conditions is in the range of 95-99 % with respect to ethylene, and the selectivity to ethylene dichloride is up to 93-96 % (Cowfer and Magistro, 1983). This exothermic reaction is catalyzed by a copper chloride catalyst impregnated on a porous alumina support. The reaction is modeled using the kinetics from a series of papers by Gel'Perin et al. (1979, 1983, 1984) described in appendix A.

3.3.1. Feed compression for oxychlorination system

The feed enters the process at low pressure (101.3 kPa) and must be compressed to a higher pressure where the reaction is feasible. For compression, we assume the choice between a single compressor

(single-stage compression), a system consisting of two compressors with intermediate cooling (two-stage compression) or a system consisting of three compressors with intermediate cooling (three-stage compression). To model the system, for the single-stage compression alternative, we define the Boolean variable Y_6 to operate at low pressure; for the two-stage compression with intermediate cooling, we define the Boolean variable Y_7 to operate at medium pressure; and for the three-stage compression with intermediate cooling, we define the Boolean variable Y_8 to operate at high pressure. We can write the following disjunction:

$$\begin{bmatrix} Y_6 \\ 152.0kPa \le P^{Comp_{OC},out} \le 202.6kPa \end{bmatrix} \vee \begin{bmatrix} Y_7 \\ 202.6kPa \le P^{Comp_{OC},out} \le 405.3kPa \\ P^{Comp\_OC,intermediate} = 202.6kPa \\ T^{Comp\_OC,intermediate} = 50^{o}C \end{bmatrix} \vee \begin{bmatrix} Y_8 \\ 405.3kPa \le P^{Comp_{OC},out} \le 1621.2kPa \\ P^{Comp\_OC,intermediate1} = 202.6kPa \\ T^{Comp\_OC,intermediate1} = 50^{o}C \\ P^{Comp\_OC,intermediate2} = 405.3kPa \\ T^{Comp\_OC,intermediate2} = 100^{o}C \end{bmatrix} \quad (7)$$

where $P^{Comp\_OC,intermediate}$ and $T^{Comp\_OC,intermediate}$ are the intermediate pressure and temperature of two-stage compression, respectively (in Figure 3, $P^{Comp\_OC,intermediate}$ corresponds with the pressure of stream leaving the compressor K-201, and $T^{Comp\_OC,intermediate}$ corresponds with the temperature of the stream leaving the heat exchanger E-200). $P^{Comp\_OC,intermediate1}$ corresponds with the pressure of stream leaving the compressor K-203, and $T^{Comp\_OC,intermediate1}$ corresponds with the temperature of the stream leaving the heat exchanger E-201. $P^{Comp\_OC,intermediate2}$ corresponds with the pressure of stream leaving the compressor K-204, and $T^{Comp\_OC,intermediate2}$ corresponds with the temperature of the stream leaving the heat exchanger E-202. $P^{Comp\_OC,out}$ is the pressure of stream leaving the feed compression system.

3.3.2. Heating/cooling before the oxychlorination reactor

The operating conditions selected in the reactor implies that the temperature of its inlet should be between 180 and 225 ºC. To get this, the resulting stream from the compressed feed has to be heated or cooled.

To model this situation, we define the Boolean variables Y_9 and Y_{10} to select a heater or a cooler, respectively.

$$\begin{bmatrix} Y_9 \\ 180^{o}C \le T^{FeedOC,out} \le 225^{o}C \\ T^{FeedOC,in} \le T^{FeedOC,out} \end{bmatrix} \vee \begin{bmatrix} Y_{10} \\ 180^{o}C \le T^{FeedOC,out} \le 225^{o}C \\ T^{FeedOC,in} \ge T^{FeedOC,out} \end{bmatrix} \quad (8)$$

where $T^{FeedOC,in}$ and $T^{FeedOC,out}$ are the temperatures entering and leaving the exchanger, respectively.

To simulate the heater (E-203), we use a heat exchanger using high-pressure steam as a hot utility. To simulate the cooler (E-204), we use a water-cooled heat exchanger using water as a refrigerant.

3.3.3. Reactor for oxychlorination

It is assumed that the reaction can take place in a PFR or in a PFR followed by a small CSTR. Note that the small CSTR could be needed for an additional conversion (Lakshmanan et al., 1999).

To model the reactor alternatives, we define the Boolean variables Y_{11} and Y_{12} to operate with a PFR or with a PFR followed by a CSTR, respectively.

$$\begin{bmatrix} Y_{11} \\ 180^{o}C \le T^{PFR,OC} \le 225^{o}C \\ 152.0kPa \le P^{PFR,OC} \le 1621.2kPa \end{bmatrix} \vee \begin{bmatrix} Y_{12} \\ 180^{o}C \le T^{PFR\_CSTR,OC} \le 225^{o}C \\ 152.0kPa \le P^{PFR\_CSTR,OC} \le 1621.2kPa \end{bmatrix} \quad (9)$$

where $T^{PFR,OC}$ is the temperature of the PFR (R-200), $P^{PFR,OC}$ is the pressure of the same reactor; $T^{PFR\_CSTR,OC}$ is the temperature of the PFR (R-201) followed by the CSTR (R-202) and $P^{PFR\_CSTR,OC}$ is the pressure of the same reactor. We have considered that if the selected option is the second one, both reactors, PFR and CSTR, operate at the same temperature and pressure conditions. The reactors are cooled using water as a refrigerant.

3.3.4. Cooling after the oxychlorination reactor

The stream leaving the oxychlorination reactor is considered to be cooled to 40 ºC in a water-cooled heat exchanger (E-205) using water as a refrigerant.

3.3.5. Separation system

The next step in the process is the separation system. The stream leaving the cooler (E-205) contains water, EDC, TCE and ethylene, HCl and unreacted O_2. First, a 3-phase separator (V-200) is used to remove water from the system. The vapor stream leaving the 3-phase separator enters to a distillation

column (T-200) where the light components (ethylene, HCl, and O_2) are obtained as the top product and recycled back to the feed compression cycle for the oxychlorination process. The column bottoms are mixed with liquid leaving the 3-phase separator. Then, a second distillation column (T-201) is added to obtain EDC as top product and TCE as a bottom product with the desired compositions. Again, a sensitivity analysis showed that the number of trays and the feed tray position had not an important impact on the total cost. Therefore, for simplicity, it was considered that the first column has 10 trays and it is fed into tray 5, and the second column has 20 trays and it is fed into tray 10.

3.4. Pyrolysis

Produced EDC during the direct chlorination and the oxychlorination stages is fed to the pyrolysis section where vinyl chloride monomer is produced (Figure 4). The pyrolysis reactor operates at 450 – 550 ºC and 202.6 – 3242.4 kPa. The conversion for the pyrolysis reaction under these conditions is 40-60 % and the selectivity to vinyl chloride is 93-100 % (Cowfer and Magistro, 1983). The kinetics of the pyrolysis reactions are compiled from various literature sources (Karra and Senkan, 1988; Kurtz, 1972; Ranzi et al., 1990; Weissman and Benson, 1984) and are described in appendix A.

The by-products recovered are recycled. Ethylene dichloride is recycled to the pyrolysis reactor and hydrogen chloride is recycled to the oxychlorination reaction section.

3.4.1. Feed heating

EDC produced in the direct chlorination is mixed with EDC produced in the oxychlorination system and EDC recycled from the separation system. This stream is considered to be heated to 200 ºC through a heat exchanger (E-300) using high-pressure steam as a hot utility.

3.4.2. Feed compression for the pyrolysis system

EDC enters the process at low pressure (101.3 kPa) and must be compressed to a higher pressure where the pyrolysis reaction is feasible. For compression, we assume the choice between a single compressor (single-stage compression), a system consisting of two compressors with intermediate cooling (two-

stage compression) or a system consisting of three compressors with intermediate cooling (three-stage compression). To model the system, for the single-stage compression alternative, we define the Boolean variable Y_{13} to operate at low pressure; for the two-stage compression with intermediate cooling, we define the Boolean variable Y_{14} to operate at medium pressure; and for the three-stage compression with intermediate cooling, we define the Boolean variable Y_{15} to operate at high pressure. We can write the following disjunction:

$$\begin{bmatrix} Y_{13} \\ 202.6kPa \le P^{Comp_{Py},out} \le 405.3kPa \end{bmatrix} \vee \begin{bmatrix} Y_{14} \\ 405.3kPa \le P^{Comp_{Py},out} \le 1621.2kPa \\ P^{Comp\_Py,intermediate} = 405.3kPa \\ T^{Comp\_Py,intermediate} = 200^{o}C \end{bmatrix} \vee \begin{bmatrix} Y_{15} \\ 1621.2kPa \le P^{Comp_{Py},out} \le 3242.4kPa \\ P^{Comp\_Py,intermediate1} = 405.3kPa \\ T^{Comp\_Py,intermediate1} = 200^{o}C \\ P^{Comp\_Py,intermediate2} = 810.6kPa \\ T^{Comp\_Py,intermediate2} = 200^{o}C \end{bmatrix} \quad (10)$$

where $P^{Comp\_Py,intermediate}$ and $T^{Comp\_Py,intermediate}$ are the intermediate pressure and temperature of two-stage compression, respectively (in Figure 4, $P^{Comp\_Py,intermediate}$ corresponds with the pressure of stream leaving the compressor K-301, and $T^{Comp\_Py,intermediate}$ corresponds with the temperature of the stream leaving the heat exchanger E-301). $P^{Comp\_Py,intermediate1}$ corresponds with the pressure of stream leaving the compressor K-303, and $T^{Comp\_Py,intermediate1}$ corresponds with the temperature of the stream leaving the heat exchanger E-302. $P^{Comp\_Py,intermediate2}$ corresponds with the pressure of stream leaving the compressor K-304, and $T^{Comp\_Py,intermediate2}$ corresponds with the temperature of the stream leaving the heat exchanger E-303. $P^{Comp\_Py,out}$ is the pressure of stream leaving the feed compression system.

3.4.3. Heating/cooling before the pyrolysis reactor

The operating conditions selected in the reactor implies that the temperature of its inlet should be between 450 and 550 ºC. To get this, the resulting stream from the compressed feed has to be heated or cooled.

To model this situation, we define the Boolean variables Y_{16} and Y_{17} to select a heater or a cooler, respectively.

$$\begin{bmatrix} Y_{16} \\ 450^{o}C \le T^{FeedPy,out} \le 550^{o}C \\ T^{FeedPy,in} \le T^{FeedPy,out} \end{bmatrix} \vee \begin{bmatrix} Y_{17} \\ 450^{o}C \le T^{FeedPy,out} \le 550^{o}C \\ T^{FeedPy,in} \ge T^{FeedPy,out} \end{bmatrix} \quad (11)$$

where $T^{FeedPy,in}$ and $T^{FeedPy,out}$ are the temperatures entering and leaving the exchanger, respectively.

To simulate the heater (E-304), we use a heat exchanger using fuel oil as a hot utility. To simulate the cooler (E-305), we use a water-cooled heat exchanger using water as a refrigerant.

3.4.4. Reactor for pyrolysis

Vinyl chloride monomer is produced by thermal cracking of EDC in a tubular reactor. A plug flow reactor (PFR) was used to model the pyrolysis section, where heat supplied to the reactor (R-300) is provided by an oven that uses fuel oil as a hot utility.

3.4.5. Cooler after the pyrolysis reactor

The stream produced in the pyrolysis reactor is cooled to obtain a liquid stream. To simulate the cooler, we use a water-cooled heat exchanger (E-306) using water as a refrigerant.

3.4.6. Separation system

The next step in the process is the separation system. The stream leaving the cooler (E-306) is first pumped before entering to the separation system, where we remove the light component (HCl) and the high component (EDC), obtaining VCM with the desired composition.

To model this situation, we have studied eight different alternative distillation column sequences for separation of vinyl chloride, hydrogen chloride and ethylene dichloride (see Figure 5). We define the Boolean variables Y_{18}, Y_{19}, Y_{20}, Y_{21}, Y_{22}, Y_{23}, Y_{24}, and Y_{25}.

a) Direct sequence (Y_{18}).
b) Direct sequence with a thermal couple (Y_{19}).
c) Indirect sequence (Y_{20}).
d) Indirect sequence with a thermal couple (Y_{21}).
e) Prefractionator (Y_{22}).
f) Prefractionator with a thermal couple (HCl-VCM) (Y_{23}).
g) Prefractionator with a thermal couple (VCM-EDC) (Y_{24}).
h) Divided Wall Column (DWC) (Y_{25}).

Note that in this case, we include a Boolean variable for each sequence instead of a separation task (a comprehensive discussion on the optimization of complex separation sequences can be found in Caballero and Grossmann (2006); (2014)). This is possible because we are considering only eight alternatives. The advantage is that we can use a conjunctive representation instead of the disjunctive approach. Therefore, we avoid all the problems related to a task representation because we consider actual distillation columns. Instead of a Kriging model, in this case, we use the Fenske-Underwood-Gilliland shortcut model (Fenske, 1932; Gilliland, 1940; Underwood, 1949), which does not introduce numerical noise, and validate each configuration with a rigorous simulation.

4. Results

The plant has been simulated on Aspen HYSYS v.8.4 in a 3.60 GHz i7-Core Processor and 8 GB of RAM under Windows 7. The UNIQUAC model is used as a thermodynamic package in the simulation. Kriging surrogate models were calibrated using MATLAB (The Mathworks, 2014). As MINLP solver, we use an implementation of the Outer Approximation (OA) (Duran and Grossmann, 1986) available through TOMLAB-MATLAB (Holmström, 1999). The complete model, objective function, explicit constraints, implicit models (models in the simulator) and surrogate models, are written in a proprietary modeling language (Caballero et al., 2014) interfaced with TOMLAB (Holmström, 1999).

First, we carry out a sensitivity analysis to determine which units have to be replaced by Kriging surrogate models and if we need or not to merge some units in a single surrogate model. The three main criteria to decide when a unit (or set of units) is substituted by a surrogate model are the large CPU convergence time, an unacceptable numerical noise, and the lack of convergence in the complete area of the domain. The reactors and distillation columns are slightly noisy; therefore, those units have been replaced by Kriging surrogate models. The rest of the unit operations, mixers, splitters, compressors, pumps, heaters, and coolers, are maintained in their original form in the process simulator.

However, if we substitute each reactor or distillation column by a Kriging surrogate model, some surrogate models will have a large number of degrees of freedom (more than 5 or 6 degrees of freedom) due to the number of components existing after the reactions. Consequently, some units have been

merged into a single metamodel. Specifically, units R-201 and R-202 have been merged into a single unit surrogate (unit R-OC). Moreover, a similar situation happens with equipment V-200, T-200, and T-201 (unit S-OC). For example, if units R-201 and R-202 are not merged into a single metamodel, the resulting surrogate model for unit R-202 would have ten independent variables, due to the amount of components produced in unit R-201. However, if we merge both reactors into unit R-OC, the number of independent variables is reduced to five. The same behavior occurs if we do not merge V-200, T-200, and T-201 into a single unit.

In a system with numerical noise, if we converge the recycles at each iteration, we must ensure that the convergence tolerance is small enough to avoid the numerical noise propagation; otherwise, recycle streams could act as <<noise amplifiers>>. Besides, the convergence of all the recycles at each iteration considerably slow down the optimization because we must converge all the units in the simulator an undetermined number of times to close the recycles with the requested accuracy. To avoid all these problems, recycles are transferred to the MINLP solver in the form of constraints. The flowsheet contains four recycle streams.

We calibrate a set of smaller surrogate models. Table 2 shows all the input-output Kriging metamodels used in this case study. Data for the Kriging models can be found in the supplementary material accompanying the paper.

Once all the Kriging models have been calibrated, it is important to validate the surrogate models. We use "cross-validation" that allows us to check the accuracy of the model without extra sampling. The main idea is to exclude one of the points and predict it back using the n-1 remaining points (Jones et al., 1998). If the number of points is not too small and there are not too many deviations, a single point has not too much influence in the Kriging and then it is not needed to reestimate the Kriging parameters. This procedure is repeated for all the points.

As an example, Figure 6 shows the results from cross-validation for VCM produced in the PFR during the pyrolysis process. From the data in Figure 6, it can be seen that the differences between the simulation model and the Kriging metamodel are minimal. Therefore, the relatively low errors of all the

Kriging metamodels in the domain of the variables, allow us to use these models instead of the simulation models.

The parameters obtained to build all the Kriging models can be found as supplementary material.

The aim of this work consists of determining the best flowsheet topology in order to maximize the profit of the process, taking into account raw material costs, operating and capital costs, and income from the sales of the by-product (TCE) and the main product (VCM).

The maximum profit obtained after the optimization is $17.0941 million/year. We achieve a maximum profit through the optimal configuration shown in Figure 7.

The optimal solution shows that the best configuration combines the direct chlorination of ethylene with the oxychlorination of ethylene in order to maximize the profit of the process. This result is comparable with the optimal superstructure obtained in the work by Turkay and Grossmann (1998). The reason for not using the direct chlorination alone is because the hydrogen chloride by-product is a toxic chemical that has a very limited market demand. This explains why in the optimal flowsheet the HCl by-product is recycled to the oxychlorination reaction section, increasing the vinyl chloride production.

Direct chlorination of ethylene is carried out using the CSTR reactor. For oxychlorination of ethylene, the three-stage compression system is used to increase the pressure of raw materials to reactor pressure. The oxychlorination reaction takes place in a PFR followed by a small CSTR. EDC obtained by direct chlorination and oxychlorination is mixed before entering a three-stage compression system, where the pressure is increased to the required pressure in the VCM reactor. Vinyl chloride monomer is separated from EDC and HCl using a prefractionator with a thermal couple.

The main characteristics of the selected equipment in the optimal solution are shown in Table 3, Table 4 and Table 5.

Mass flows and prices of raw materials and products obtained are shown in Table 6.

In this paper, we have built a large number of Kriging models with a low number of degrees of freedom (maximum 5 independent variables). Surrogate models with more independent variables tend to be less accurate and require a very large number of training points (Quirante et al., 2015).

The MINLP model is solved in 15 min 41 s.

The methodology followed has proven to be accurate and reliable to solve hybrid models, which include process flowsheet at the level of commercial process simulator, Kriging surrogate models, and explicit equations (Quirante and Caballero, 2016). In this case, we have shown that the methodology can be easily extended to the case when the topology is not fixed.

4.1. Energy integration of the process flowsheet

Heat integration is the most effective method to reduce costs, through thermal integration between heating and cooling systems. The Heat Exchanger Network (HEN) is a basic component in the most of the industrial processes because they can significantly contribute to decreasing energy consumption (Allen et al., 2009). Therefore, in order to improve the energy efficiency of the plant, the heat exchanger network of the VCM process has been designed.

The heat content of the reactor streams may be used to heat the cold streams. The process has fifteen hot process streams (H1 – H15) and nine cold process streams (C1 – C9). Following the solution obtained from the optimal process, the temperatures and the heat capacity flowrates are used to get a heat exchanger network (HEN). To determine the optimal HEN we have followed the MINLP formulation proposed by Yee and Grossmann (1990). A minimum approach temperature (ΔT_{ml}) of 10 ^{o}C is assumed for an efficient heat exchanger.

Data of the streams involved in the heat integration are shown in Table 7.

The profit obtained prior to the heat integration is $17.0941 million/year, and the profit obtained after the heat integration is raised to $18.7971 million/year. Table 8 summarizes the utility needed on the economically optimized plant and on the heat integrated plant.

Table 8 shows that utility consumptions are considerably reduced in the heat integrated process. The HEN reduces heating and cooling requirements (66.8 % and 26.3 %, respectively), what implies a reduction in the corresponding operating costs.

Finally, the HEN has been generated using the superstructure approach proposed by Yee and Grossmann (1990). Figure 8 shows the heat exchanger network.

In addition, several studies have shown that a reduction of energy consumption can accomplish the minimization of environmental impacts (Lara et al., 2013; Morar and Agachi, 2010).

4.2. Economic feasibility study

The optimization of the VCM process has been performed using deterministic values of the raw materials, products and utility prices given in Table 1. However, in this section, we check the economic feasibility of the optimized and heat integrated process in a more rigorous way. To this end, the inherent uncertainty in the raw material and product prices are taken into account. Assuming uncertainty in the prices provides robust results as opposed to the deterministic ones, based on nominal values. The objective of this study is not to optimize the flowsheet by introducing uncertainty in the prices, but it is to study how a change in the prices could influence in achieving the desired profit.

To assess the benefits from the optimal process assuming a level of uncertainty in the prices, various metrics may be employed. For our purposes, the concept of financial risk is used.

The financial risk is a probabilistic approach to risk management defined as the probability of not meeting a certain target value, Ω (Barbaro and Bagajewicz, 2004). In the framework of the present economic study, the financial risk is referred as the probability of not meeting the desired profit with

our optimal VCM process. The financial risk (*FRisk*) associated with our VCM flowsheet, *x*, and a target value, Ω, is given by Eq.(12).

$$FRisk(x,\Omega) = P\left[Profit(x) < \Omega\right] \tag{12}$$

where *Profit(x)* is the actual profit (the resulting profit after introducing the uncertainty). Because a finite number of independent scenarios represents uncertainty in the raw material and product prices, the financial risk can be defined in terms of the probability of not meeting the target value in each scenario *s*.

$$FRisk(x,\Omega) = \sum_{s\in S} P\left[Profit_s(x) < \Omega\right] \tag{13}$$

In addition, for each particular scenario, the profit is either greater (or equal) than the target value, in which case the probability is zero, or smaller than the target when the probability is one. Therefore, the financial risk can be expressed as Eq.(14).

$$FRisk(x,\Omega) = \sum_{s\in S} \omega_s Z_s(x,\Omega) \tag{14}$$

where ω_s is the probability of scenario, generally taken as $1/|S|$, where $|S|$ is the cardinality of the set of scenarios; and $Z_s(\Omega)$ is a binary variable defined for each scenario (see Eq.(15)).

$$Z_s(x,\Omega) = \begin{cases} 1 \;\; if \;\; Profit_s(x) < \Omega \\ 0 \;\; otherwise \end{cases} \qquad \forall s \in S \tag{15}$$

The profit achieved with the process is calculated through Eq.(16).

$$Profit_s(MM\$/year) = Income_s - Costs_s - TAC \tag{16}$$

Each term of Eq.(16) is given by Eq.(17).

$$\begin{aligned} &Income_s(MM\$/year) = VCM\ Sales_s + TCE\ Sales_s \\ &Costs_s(MM\$/year) = Ethylene\ Cost_s + Cl_2\ Cost_s + HCl\ Cost_s + O_2\ Cost_s \\ &TAC(MM\$/year) = Operating\ cost + F\cdot Capital\ cost \end{aligned} \tag{17}$$

A critical issue in this methodology is the generation of appropriate values of the uncertain parameters. In this work, we model the uncertainty in the raw material and product prices by a set of scenarios, generated by Monte Carlo sampling (Marsaglia and Tsang, 2000).

There is a broad family of probability distribution functions. Some of the most common ones are the normal, uniform, triangular and lognormal distributions. In this case, we have selected the triangular

distribution for the generation of the different scenarios. This distribution is typically used in economic simulations and provides a good representation of the probability distribution for the uncertain prices when limited sample data is available (The Mathworks, 2014). Parameters for triangular distribution are the minimum price *a*, the maximum price *b*, and the most likely price *c*.

Data prices for raw materials, products, and utilities are shown in Table 9 (updated values to 2015) (ICIS, 2015).

The parameters of the triangular distribution *a*, *b* and *c* are obtained from this data. The parameters *a* and *b* are obtained from Table 9, decreasing and increasing the minimum and maximum prices by 10 % respectively. And the most likely price *c* is estimated from the sample mean. The results are shown in Table 10.

The expected value *E[X]*, variance *Var[X]* and standard deviation *sd[X]* of the triangular probability distribution function are obtained through the following expressions (see Table 11):

$$E[X] = \frac{a+b+c}{3}$$
$$Var[X] = \frac{a^2+b^2+c^2-ab-ac-bc}{18} \quad (18)$$
$$sd[X] = \sqrt{Var[X]}$$

The more direct way to assess the trade-offs between risk and the potential profit of the proposed VCM process is to use the cumulative risk curve. For the given process, this curve shows the level of incurred financial risk at each potential profit level. Therefore, the cumulative curve is obtained when the financial risk of a set of different targets Ω is computed and plotted. Figure 9 shows the cumulative risk curve for the optimal and heat integrated VCM process for a set of expected profits ranging from 0 to 30 million dollars per year.

The curve of Figure 9 shows that the optimal profit obtained after the heat integration ($18.7911 million/year) is found for an incurred financial risk around 55.9 %. In addition, as a reference value, the configuration obtained can achieve a potential profit of $12.2 million/year with a financial risk of not achieving the target value of 5 %.

5. Conclusions

In this paper, we have dealt with hybrid models involving process simulators and explicit constraints. The problem that certain simulation modules present is that they can be slightly noisy or difficult to converge. In this work, this problem has been addressed by combining process simulators and surrogate models based on Kriging interpolation. Additionally, some parts of the model were aggregated in order to reduce the degrees of freedom of the Kriging surrogate models, allowing us to increase the robustness of the optimization model. Therefore, the final model was composed of unit operations maintained in the simulator, Kriging surrogate models, and explicit equations.

As a case study, the optimization of the benchmark vinyl chloride monomer production process has been proposed to demonstrate the robustness of the proposed approach. The process consists of three reaction sections: direct chlorination (CSTR), oxychlorination (PFR + CSTR) and pyrolysis (PFR).

This approach can be used to synthesize any chemical process using a superstructure optimization-based approach. Once the alternatives have been selected and the superstructure generated, the great advantage of the proposed approach is that the solution is a feasible flowsheet (at least a locally optimal solution) generated using state-of-the-art models (e.g., those implemented in a commercial process simulator or any other proprietary software).

The direct industrial implementation depends on which is the confidence of the designer in the model. The approach could be used always but is the designer who decides the level of complexity of the models to balance rigorousness with numerical efficiency. However, this is out of the scope of the paper. We propose a framework that allows using the best available model(s) –rigorous thermodynamics, transport equations, etc.– for synthesizing chemical processes.

Energy integration of the process flowsheet was also performed to determine the minimum utility consumption of the process, obtaining the heat exchanger network. This allows us a significant cost saving, with the consequent reduction of the environmental impacts.

The financial risk was also studied. The optimal configuration obtained can achieve a potential profit of \$12.2 million/year with a financial risk of not achieving the target value around 5 %.

It has been shown that the proposed method is very effective, efficient and robust for structural flowsheet optimization problems.

Acknowledgements

The authors gratefully acknowledge the financial support by the Ministry of Economy and Competitiveness from Spain, under the project CTQ2016-77968-C3-02-P (AEI/FEDER, UE), and Call 2013 National Sub-Program for Training, Grants for pre-doctoral contracts for doctoral training (BES-2013-064791).

Appendix A. Kinetic schemes for the reaction sections in the vinyl chloride monomer production

A.1. Direct chlorination reaction kinetics

The kinetics for direct chlorination of ethylene to EDC were derived from Wachi and Morikawa (1986). EDC and trichloroethane (TCE) are formed through molecular addition and substitution reactions.

Reaction DC1:

$$C_2H_4 + Cl_2 \xrightarrow{k_1} C_2H_4Cl_2$$

$$R_1 = k_1[C_2H_4][Cl_2]$$

$$k_1 = 3.1040 \cdot 10^{17} \exp\left(-\frac{96930}{RT}\right) \qquad \left(\frac{m^3}{kmol \cdot s}\right)$$

Reaction DC2:

$$C_2H_4Cl_2 + Cl_2 \xrightarrow{k_2} C_2H_3Cl_3 + HCl$$

$$R_2 = k_2[C_2H_4Cl_2][Cl_2]$$

$$k_2 = 1.7460 \cdot 10^{17} \exp\left(-\frac{100980}{RT}\right) \qquad \left(\frac{m^3}{kmol \cdot s}\right)$$

A.2. Oxychlorination reaction kinetics

The kinetics for oxychlorination of ethylene to EDC were derived from a series of papers by Gel'Perin et al. (1979, 1983, 1984). EDC and several byproducts are formed by the following reactions.

Reaction OC1:

$$C_2H_4 + HCl + 0.5O_2 \xrightarrow{k_1} C_2H_4Cl_2 + H_2O$$
$$k_1 = 15848.9 \exp\left(-\frac{40100}{RT}\right) \qquad \left(\frac{mol}{L\ cat{\cdot}h{\cdot}kPa^{1.5}}\right)$$
$$r_{C_2H_4} = k_1 p_{C_2H_4} p_{Cl_2}^{0.5}$$

Reaction OC2:

$$C_2H_4Cl_2 + HCl + 0.5O_2 \xrightarrow{k_2} C_2H_3Cl_3 + H_2O$$
$$k_2 = 1.6982{\cdot}10^{13} \exp\left(-\frac{128040}{RT}\right) \qquad \left(\frac{mol}{L\ cat{\cdot}h{\cdot}kPa^{1.5}}\right)$$
$$r_{C_2H_4Cl_2} = k_2 p_{C_2H_4Cl_2} p_{Cl_2}^{0.5}$$

Reaction OC3:

$$C_2H_4 + 3O_2 \xrightarrow{k_3} 2CO_2 + H_2O$$
$$k_3 = 6.0256{\cdot}10^{6} \exp\left(-\frac{112000}{RT}\right) \qquad \left(\frac{mol}{L\ cat{\cdot}h{\cdot}kPa^{2.5}}\right)$$
$$r_{C_2H_4}^{ox} = k_3 p_{O_2} p_{Cl_2}^{0.5} p_{C_2H_4}$$

Reaction OC4:

$$4HCl + O_2 \xrightarrow{k_4} 2Cl_2 + 2H_2O$$
$$k_4 = 1.2424{\cdot}10^{8} \exp\left(-\frac{121342}{RT}\right) \qquad \left(\frac{mol}{L\ cat{\cdot}h}\right)$$
$$r_{Cl_2} = k_4 p_{O_2} p_{Cl_2}^{-1}$$

A.3. Pyrolysis reaction kinetics

The kinetics for the pyrolysis of EDC to vinyl chloride monomer were compiled from various literature sources (Karra and Senkan, 1988; Kurtz, 1972; Ranzi et al., 1990; Weissman and Benson, 1984). Vinyl chloride, HCl, and EDC are the main products formed through the following reactions.

Reaction P1:

$$1,2C_2H_4Cl_2 \xrightarrow{k_1} C_2H_3Cl + HCl$$
$$k_1 = 3.6{\cdot}10^{13} \exp\left(-\frac{242683}{RT}\right) \qquad \left(s^{-1}\right)$$

Reaction P2:

$$C_2H_3Cl \xrightarrow{k_2} C_2H_2 + HCl$$
$$k_2 = 5.0 \cdot 10^{13} \exp\left(-\frac{288710}{RT}\right) \qquad \left(s^{-1}\right)$$

Reaction P3:

$$1,2C_2H_4Cl_2 \xrightarrow{k_3} C_2H_4 + Cl_2$$
$$k_3 = 1.0 \cdot 10^{13} \exp\left(-\frac{301262}{RT}\right) \qquad \left(s^{-1}\right)$$

References

Allen, B., Savard-Goguen, M., Gosselin, L., 2009. Optimizing heat exchanger networks with genetic algorithms for designing each heat exchanger including condensers. Appl Therm Eng 29, 3437-3444.

Aspelund, A., Gundersen, T., Myklebust, J., Nowak, M.P., Tomasgard, A., 2010. An optimization-simulation model for a simple LNG process. Comput Chem Eng 34, 1606-1617.

Aspen Technology, I., 1994-2015. Aspen Technology, Inc. Aspen HYSYS 8.8. Aspen Plus.

Balas, E., 1979. Disjunctive Programming, in: Hammer, P.L., Johnson, E.L., Korte, B.H. (Eds.), Annals of Discrete Mathematics. Elsevier, Canada, pp. 3-51.

Barbaro, A., Bagajewicz, M.J., 2004. Managing financial risk in planning under uncertainty. AIChE J 50, 963-989.

Biegler, L.T., Lang, Y.D., Lin, W., 2014. Multi-scale optimization for process systems engineering. Comput Chem Eng 60, 17-30.

Bravo-Bravo, C., Segovia-Hernández, J.G., Gutiérrez-Antonio, C., Durán, A.L., Bonilla-Petriciolet, A., Briones-Ramírez, A., 2010. Extractive Dividing Wall Column: Design and Optimization. Ind Eng Chem Res 49, 3672-3688.

Brunet, R., Reyes-Labarta, J.A., Guillén-Gosálbez, G., Jiménez, L., Boer, D., 2012. Combined simulation–optimization methodology for the design of environmental conscious absorption systems. Comput Chem Eng 46, 205-216.

Caballero, J.A., Grossmann, I.E., 2006. Structural considerations and modeling in the synthesis of heat-integrated-thermally coupled distillation sequences. Ind Eng Chem Res 45, 8454-8474.

Caballero, J.A., Grossmann, I.E., 2008. An algorithm for the use of surrogate models in modular flowsheet optimization. AIChE J 54, 2633-2650.

Caballero, J.A., Grossmann, I.E., 2014. Optimal synthesis of thermally coupled distillation sequences using a novel MILP approach. Comput Chem Eng 61, 118-135.

Caballero, J.A., Milán-Yañez, D., Grossmann, I.E., 2005. Rigorous design of distillation columns: Integration of disjunctive programming and process simulators. Ind Eng Chem Res 44, 6760-6775.

Caballero, J.A., Navarro, M.A., Ruiz-Femenia, R., Grossmann, I.E., 2014. Integration of different models in the design of chemical processes: Application to the design of a power plant. Appl Energy 124, 256-273.

Chen, Y., Eslick, J., Grossmann, I., Miller, D., 2014. Simultaneous Optimization and Heat Integration Based on Rigorous Process Simulations, in: Eden, M.R., Siirola, J.D., Towler, G.P. (Eds.), Computer Aided Chemical Engineering. Elsevier, Auburn University, AL, USA, pp. 477-482.

Conn, A., Scheinberg, K., Vicente, L.N., 2009. Introduction to Derivative-Free Optimization. Society for Industrial and Applied Mathematics (SIAM), Philadelphia, PA, USA.

Cowfer, J.A., Magistro, A.J., 1983. Vinyl chloride, in: Grayson, M., Eckroth, D. (Eds.), Kirk-Othmer Encyclopedia of Chemical Technology, 3rd ed. Wiley-Interscience, New York, pp. 865-885.

Dantus, M.M., High, K.A., 1999. Evaluation of waste minimization alternatives under uncertainty: a multiobjective optimization approach. Comput Chem Eng 23, 1493-1508.

Davis, E., Ierapetritou, M., 2007. A kriging method for the solution of nonlinear programs with black-box functions. AIChE J 53, 2001-2012.

Díaz, M.S., Bandoni, J.A., 1996. A mixed integer optimization strategy for a large scale chemical plant in operation. Comput Chem Eng 20, 531-545.

Diwekar, U.M., Grossmann, I.E., Rubin, E.S., 1992. An MINLP process synthesizer for a sequential modular simulator. Ind Eng Chem Res 3, 313-322.

Douglas, J.M., 1985. A Hierarchical Decision Procedure for Process Synthesis AIChE J 30, 353-362.

Douglas, J.M., 1988. Conceptual Design of Chemical Processes. McGraw-Hill, New York.

Duran, M.A., Grossmann, I.E., 1986. An outer-approximation algorithm for a class of mixed-integer nonlinear programs. Math Program 36, 307-339.

Eslick, J.C., Miller, D.C., 2011. A multi-objective analysis for the retrofit of a pulverized coal power plant with a CO2 capture and compression process. Comput Chem Eng 35, 1488-1500.

Fenske, M.R., 1932. Fractionation of Straight-Run Pennsylvania Gasoline. Industrial & Engineering Chemistry 24, 482-485.

Fischer, I., Schmitt, W.F., Porth, H.C., Allsopp, M.W., Vianello, G., 2014. Poly(Vinyl Chloride), Ullmann's Encyclopedia of Industrial Chemistry, pp. 1-30.

Gel'Perin, E.I., Bakshi, Y.M., Avetisov, A.K., Gel'bshtein, A.I., 1979. Kinetic model of the oxidative chlorination of ethane to vinyl chloride II. Kinetika I Kataliz 20, 129-135.

Gel'Perin, E.I., Bakshi, Y.M., Avetisov, A.K., Gel'bshtein, A.I., 1983. Kinetic model of the oxidative chlorination of ethane to vinyl chloride III. Kinetika I Kataliz 24, 633-638.

Gel'Perin, E.I., Bakshi, Y.M., Avetisov, A.K., Gel'bshtein, A.I., 1984. Kinetic model of the oxidative chlorination of ethane to vinyl chloride IV. Kinetika I Kataliz 25, 842-849.

Gilliland, E.R., 1940. Multicomponent Rectification Estimation of the Number of Theoretical Plates as a Function of the Reflux Ratio. Industrial & Engineering Chemistry 32, 1220-1223.

Gross, B., Roosen, P., 1998. Total process optimization in chemical engineering with evolutionary algorithms. Comput Chem Eng 22, S229-S236.

Grossmann, I.E., 1985. Mixed-integer programming approach for the synthesis of integrated process flowsheets. Comput Chem Eng 9, 463-482.

Grossmann, I.E., Trespalacios, F., 2013. Systematic modeling of discrete-continuous optimization models through generalized disjunctive programming. AIChE J 59, 3276-3295.

Gutiérrez-Antonio, C., Briones-Ramírez, A., 2009. Pareto front of ideal Petlyuk sequences using a multiobjective genetic algorithm with constraints. Comput Chem Eng 33, 454-464.

Henao, C.A., Maravelias, C.T., 2011. Surrogate-based superstructure optimization framework. AIChE J 57, 1216-1232.

Holmström, K., 1999. The TOMLAB optimization environment in Matlab. Adv Model Optim 1, 47-69.

ICIS, 2015. ICIS: Indicative Chemical Prices

Javaloyes-Antón, J., Ruiz-Femenia, R., Caballero, J.A., 2013. Rigorous Design of Complex Distillation Columns Using Process Simulators and the Particle Swarm Optimization Algorithm. Ind Eng Chem Res 52, 15621-15634.

Jones, D.R., 2001. A taxonomy of global optimization methods based on response surfaces. J Glob Optim 21, 345-383.

Jones, D.R., Schonlau, M., Welch, W.J., 1998. Efficient global optimization of expensive black-box functions. J Glob Optim 13, 455-492.

Karra, S.B., Senkan, S.M., 1988. A detailed chemical kinetic mechanism for the oxidative pyrolysis of CH3Cl. Ind Eng Chem Res 27, 1163-1168.

Kleijnen, J.P.C., 2009. Kriging metamodeling in simulation: A review. Eur J Oper Res 192, 707-716.

Krige, D.G., 1951. A statistical approach to some mine valuation and allied problems on the Witwatersrand, [Master's thesis]. South Africa: University of Witwatersrand.

Kurtz, B.E., 1972. Homogeneous kinetics of methyl chloride chlorination. Ind Eng Chem Res 11, 332-338.

Lakshmanan, A., Rooney, W.C., Biegler, L.T., 1999. A case study for reactor network synthesis: the vinyl chloride process. Comput Chem Eng 23, 479-495.

Lara, Y., Lisbona, P., Martínez, A., Romeo, L.M., 2013. Design and analysis of heat exchanger networks for integrated Ca-looping systems. Appl Energy 111, 690-700.

Leboreiro, J., Acevedo, J., 2004. Processes synthesis and design of distillation sequences using modular simulators: a genetic algorithm framework. Comput Chem Eng 28, 1223-1236.

Marsaglia, G., Tsang, W.W., 2000. The ziggurat method for generating random variables. J Stat Softw 5, 1-7.

McPherson, R.W., Starks, C.M., Fryar, G.I., 1979. Vinyl chloride monomer... What you should know. Hydrocarb Process 58, 75-88.

Modler, R., Willhalm, R., Yoshida, Y., 2015. Chemical Economics Handbook (CEH). SRI International, Colorado, USA.

Morar, M., Agachi, P.S., 2010. Review: Important contributions in development and improvement of the heat integration techniques. Comput Chem Eng 34, 1171-1179.

Navarro-Amorós, M.A., Ruiz-Femenia, R., Caballero, J.A., 2014. Integration of modular process simulators under the Generalized Disjunctive Programming framework for the structural flowsheet optimization. Comput Chem Eng 67, 13-25.

Nemhauser, G.L., Wolsey, L.A., 1988. Integer and combinatorial optimization. John Wiley & Sons, Inc, New York.

Odjo, A.O., Sammons, N.E., Yuan, W., Marcilla, A., Eden, M.R., Caballero, J.A., 2011. Disjunctive-Genetic Programming Approach to Synthesis of Process Networks. Ind Eng Chem Res 50, 6213-6228.

Palmer, K., Realff, M., 2002a. Metamodeling approach to optimization of steady-state flowsheet simulations. Chem Eng Res Des 80, 760-772.

Palmer, K., Realff, M., 2002b. Optimization and Validation of Steady-State Flowsheet Simulation Metamodels. Chem Eng Res Des 80, 773-782.

Quirante, N., Caballero, J.A., 2016. Large scale optimization of a sour water stripping plant using surrogate models. Comput Chem Eng 92, 143-162.

Quirante, N., Javaloyes, J., Caballero, J.A., 2015. Rigorous design of distillation columns using surrogate models based on Kriging interpolation. AIChE J 61, 2169-2187.

Raman, R., Grossmann, I.E., 1994. Modelling and computational techniques for logic based integer programming. Comput Chem Eng 18, 563-578.

Ranzi, E., Dente, M., Tiziano, F., Mullick, S., Bussani, G., 1990. Mechanistic modeling of chlorinated reacting systems. Chimica e l'Industria 72, 905.

Reneaume, J.-M.F., Koehret, B.M., Joulia, X.L., 1995. Optimal Process Synthesis in a Modular Simulator Environment: New Formulation of the Mixed-Integer Nonlinear Programming Problem. Ind Eng Chem Res 34, 4378-4394.

Sacks, J., Welch, W.J., Mitchell, T.J., Wynn, H.P., 1989. Design and Analysis of Computer Experiments. Stat Sci 4, 409-423.

Shao, T., Krishnamurty, S., Wilmes, G.C., 2007. Preference-based surrogate modeling in engineering design. AIAA Journal 45, 2688-2701.

Smith, R., 2005. Chemical process: Design and integration. Jonh Wiley & Sons, Chichester.

The Mathworks, I., 2014. The Mathworks, Inc. Matlab 8.3. Natick, MA: The Mathworks, Inc.

Turkay, M., Grossmann, I.E., 1996. Logic-based MINLP algorithms for the optimal synthesis of process networks. Comput & Chem Eng 20, 959-978.

Turkay, M., Grossmann, I.E., 1998. Structural flowsheet optimization with complex investment cost functions Comput & Chem Eng 22, 673-686.

Turton, R., Bailie, R.C., Whiting, W.B., Shaeiwitz, J.A., 2013. Analysis, synthesis, and design of chemical processes, 4th ed. Prentice Hall, Upper Saddle River, New Jersey.

Underwood, A.J.V., 1949. Fractional Distillation of Multicomponent Mixtures. Industrial & Engineering Chemistry 41, 2844-2847.

Vazquez–Castillo, J.A., Venegas–Sánchez, J.A., Segovia–Hernández, J.G., Hernández-Escoto, H., Hernández, S., Gutiérrez–Antonio, C., Briones–Ramírez, A., 2009. Design and optimization, using genetic algorithms, of intensified distillation systems for a class of quaternary mixtures. Comput Chem Eng 33, 1841-1850.

Wachi, S., Morikawa, H., 1986. Liquid phase chlorination of ethylene and 1,2-Dichloroethane. J Chem Eng Jpn 19, 437-443.

Weissman, M., Benson, S.W., 1984. Pyrolysis of methyl chloride, a pathway in the chlorine-catalyzed polymerization of methane. Int J Chem Kinet 16, 307-333.

Won, K.S., Ray, T., 2005. A framework for design optimization using surrogates. Eng Optim 37, 685-703.

Xiong, Y., Chen, W., Apley, D., Ding, X., 2007. A non-stationary covariance-based Kriging method for metamodelling in engineering design. Int J Numer Meth Eng 71, 733-756.

Yee, T.F., Grossmann, I.E., 1990. Simultaneous optimization models for heat integration - II. Heat exchanger network synthesis. Comput Chem Eng 14, 1165-1184.

Yeomans, H., Grossmann, I.E., 1999. A systematic modeling framework of superstructure optimization in process synthesis. Comput Chem Eng 23, 709-731.

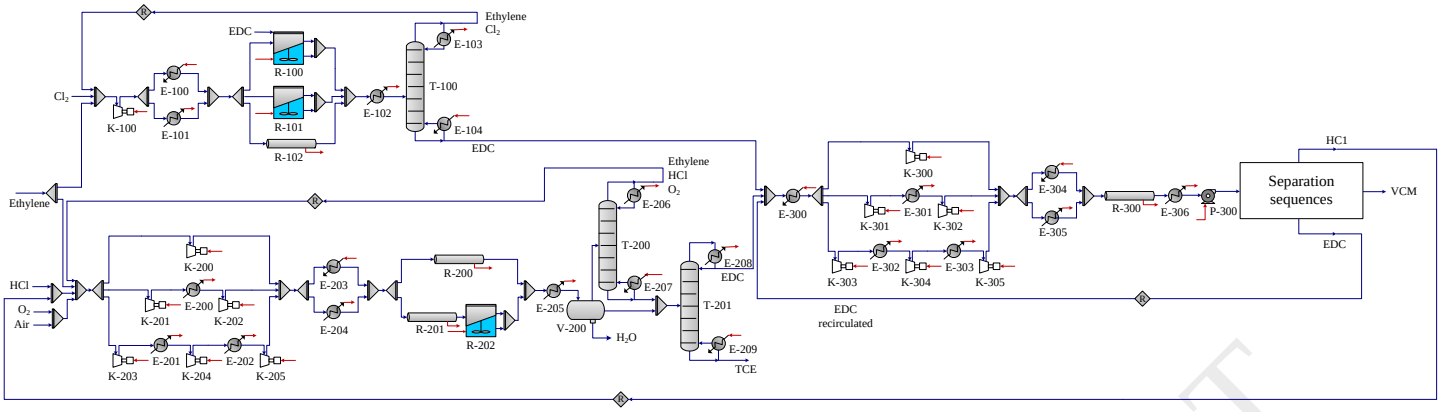

Figure 1. Superstructure for the vinyl chloride monomer production.

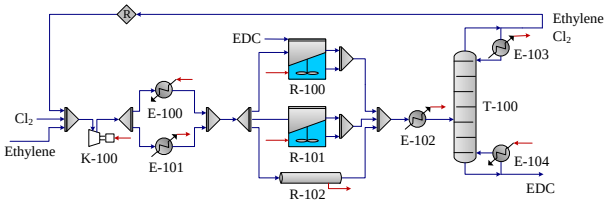

Figure 2. Superstructure for the direct chlorination of ethylene.

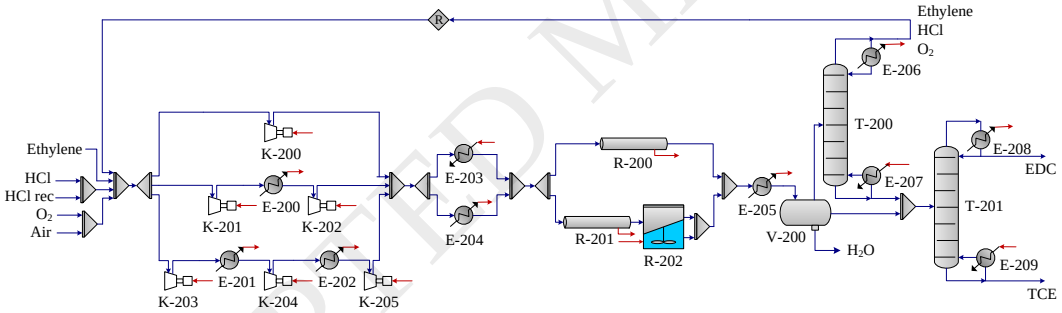

Figure 3. Superstructure for the oxychlorination of ethylene.

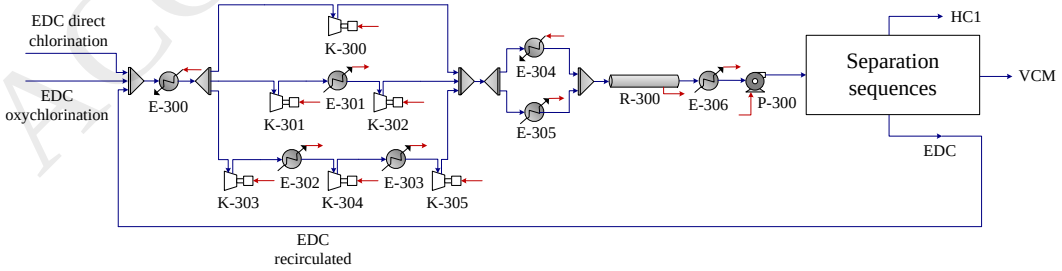

Figure 4. Superstructure for the pyrolysis of EDC.

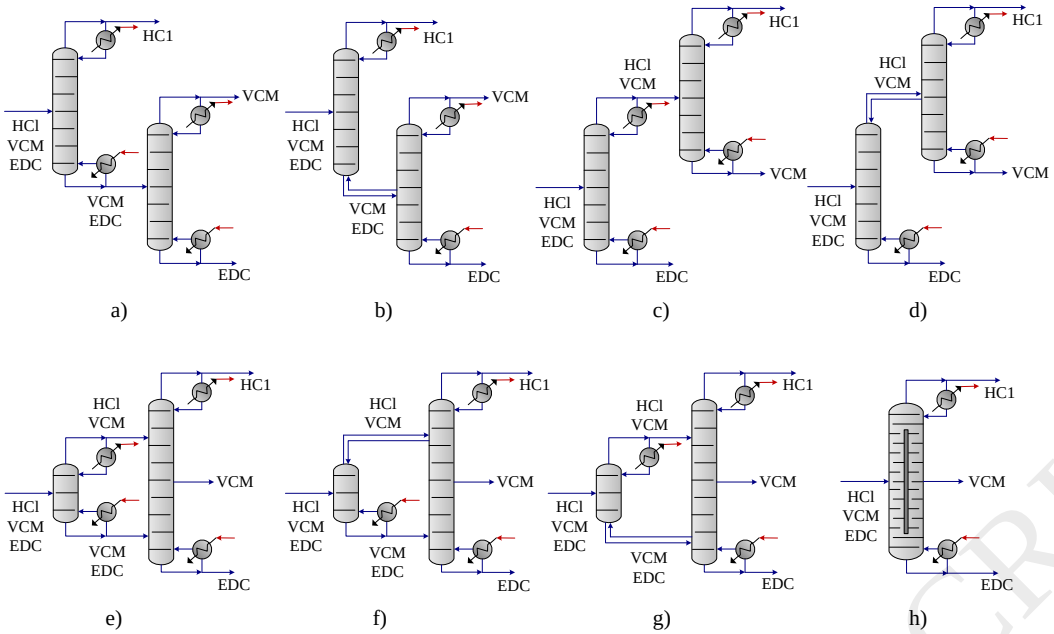

Figure 5. Eight separation configurations represented in Figure 4 as "separation sequences". Notation: Hydrochloric acid (HCl), Vinyl Chloride Monomer (VCM), Ethylene Dichloride (EDC).

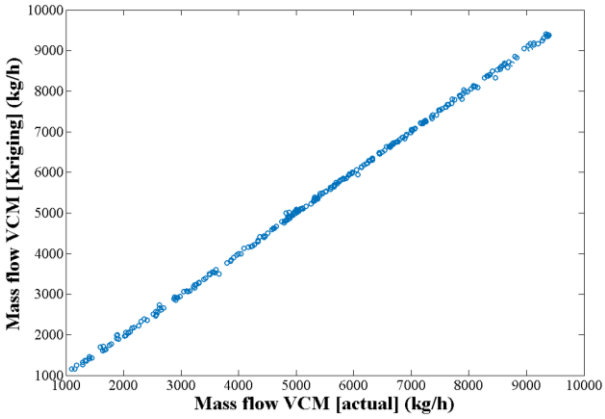

Figure 6. Cross-validation for VCM produced in the pyrolysis reactor.

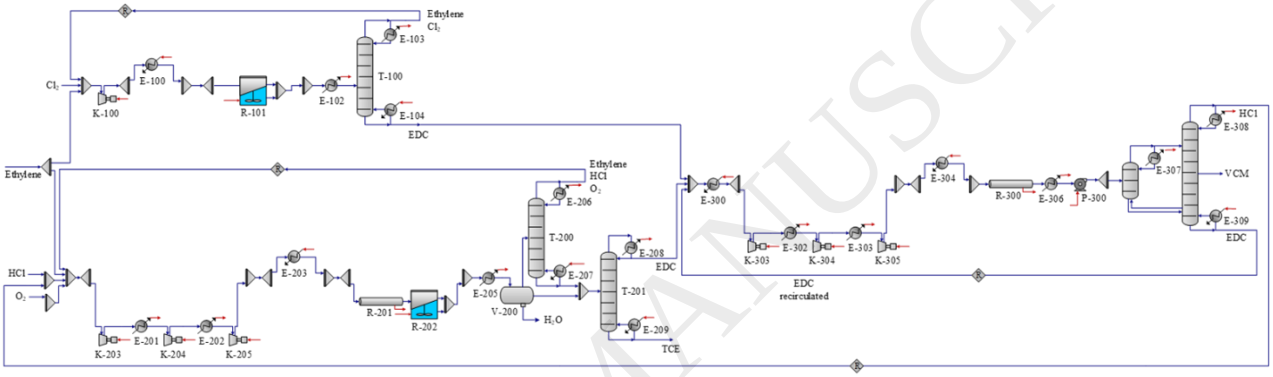

Figure 7. Optimized flowsheet for the production of vinyl chloride monomer.

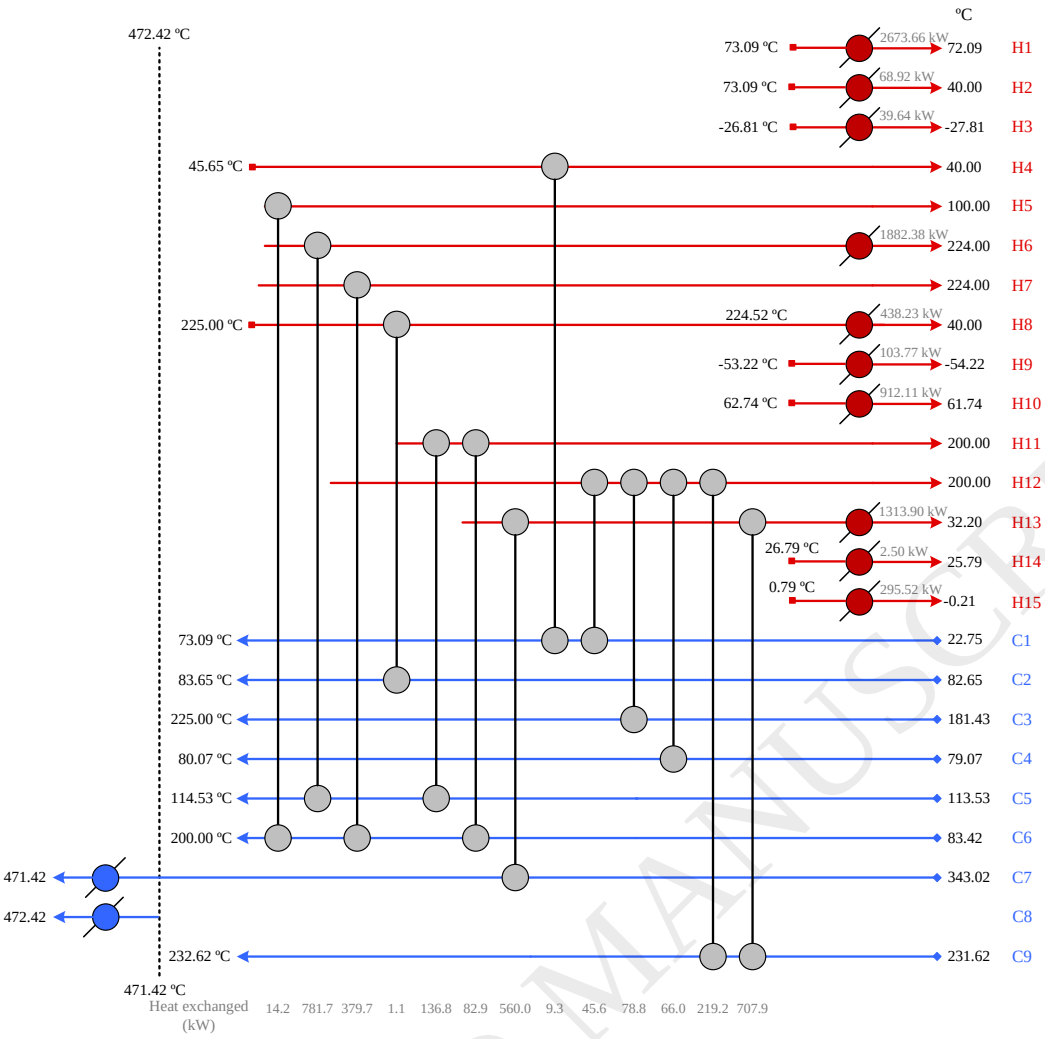

Figure 8. Heat exchanger network of the VCM plant.

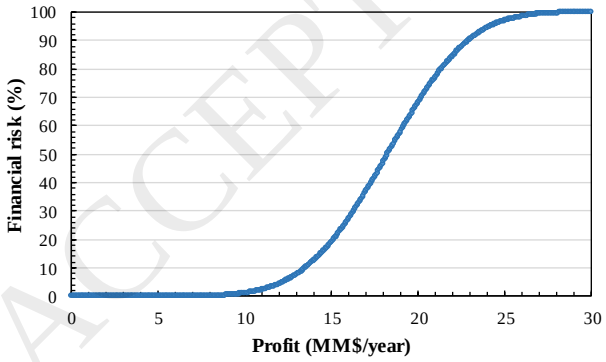

Figure 9. Cumulative risk curve.

Table 1. Prices of the raw materials, products, and utilities.

Raw material /Product	**Cost ($/kg)**	**Utility**	**Cost ($/kWh)**
Ethylene	1.2802	Refrigerants	
Cl_2	0.2578	Cooling water (30ºC to 40ºC)	0.0013
HCl	0.0855	Refrigerant (refrigerated water 5ºC)	0.0159
O_2	0.0416	Refrigerant (low temperature -20ºC)	0.0284
		Refrigerant (very low temperature -50ºC)	0.0472
VCM	0.7505	Refrigerant (extremely low temperature -100ºC)	0.0900
TCE	1.1920	Electricity	0.0600
		Steam from boilers	
		LP steam (500 kPa, 160ºC)	0.0506
		HP steam (4100 kPa, 254ºC)	0.0637
		Fuel oil	0.0511

Table 2. Input-output Kriging metamodels used in the case study.

	Inputs	**Outputs**
R-101	Temperature Pressure Mass flow (ethylene, Cl_2)	Mass flow (ethylene, Cl_2, EDC) Heat flow
T-100	Temperature Pressure Mass flow (ethylene, Cl_2, EDC)	Mass flow (distillate [ethylene, Cl_2], bottom [EDC]) Temperature (distillate, bottom) Heat flow (E-103, E-104) Diameter
R-OC	Temperature Pressure Mass flow (ethylene, HCl, O_2)	Mass flow (ethylene, HCl, O_2, EDC, TCE, H_2O) Heat flow (R-201, R-202)
S-OC	Temperature Pressure Mass flow (ethylene, HCl, O_2)	Mass flow (distillate [ethylene, HCl, O_2]) Mass flow (distillate [EDC], bottom [TCE]) Mass flow H_2O Temperature distillate (T-200, T-201) Temperature bottom (T-200, T-201) Heat flow (E-203, E-204, E-205, E-206) Diameter (T-200, T-201)
R-300	Temperature Pressure Mass flow (EDC)	Mass flow (HCl, EDC, VCM) Heat flow

Table 3. Main characteristics of equipment selected in direct the chlorination system.

Compressor (K-100)		**Heater (E-100)**	
Type	Single-stage compression	**Type**	Heater
Inlet pressure (kPa)	101.3250	Area (m^2)	0.7238
Outlet pressure (kPa)	101.3250	Inlet temperature (ºC)	22.7518
Power (kW)	0.0000	Outlet temperature (ºC)	73.0941
		Utility	LP steam
Cost		**Cost**	
Annualized capital cost ($MM/year)	0.0000	Annualized capital cost ($MM/year)	0.0235
Electricity cost ($MM/year)	0.0000	Utility cost ($MM/year)	0.0265
Reactor (R-101)		**Cooler (E-102)**	
Type	CSTR	**Type**	Cooler
Volume (m^3)	50.0000	Area (m^2)	1.6963
Utility	Water	Inlet temperature (ºC)	73.0941
Energy (kW)	3192.3029	Outlet temperature (ºC)	40.0000
		Utility	Water
Cost		**Cost**	
Annualized capital cost ($MM/year)	0.1063	Annualized capital cost ($MM/year)	0.0184
Utility cost ($MM/year)	0.0325	Utility cost ($MM/year)	0.0079
Column (T-100)			
Condenser		**Reboiler**	
Area (m^2)	1.6963	Area (m^2)	1.7808
Temperature distillate (ºC)	-26.8069	Temperature distillate (ºC)	82.6478
Utility	Refrigerant	Utility	LP steam
Cost		**Cost**	
Annualized capital cost ($MM/year)	0.0668	Annualized capital cost ($MM/year)	0.0435
Utility cost ($MM/year)	0.0071	Utility cost ($MM/year)	0.0457
Trays and tower			
Material of construction	Carbon steel	Number of trays [N_t]	10.0000
Tray spacing (m)	$H_t = 0.6096$	Diameter (m)	0.3016
Column height (m)	$H = 3 + N_t \cdot H_t$	Annualized capital cost ($MM/year)	0.0055

Table 4. Main characteristics of equipment selected in the oxychlorination system.

Compression system			
Type	Three-stage compression		
Compressor (K-203)		**Cooler (E-201)**	
Inlet pressure (kPa)	101.3250	Area (m^2)	0.3455
Outlet pressure (kPa)	202.6500	Inlet temperature (ºC)	45.6500
Power (kW)	91.5638	Outlet temperature (ºC)	40.0000
		Utility	Water
Cost		**Cost**	
Annualized capital cost ($MM/year)	0.0266	Annualized capital cost ($MM/year)	0.0317
Electricity cost ($MM/year)	0.0440	Utility cost ($MM/year)	0.0012
Compressor (K-204)		**Cooler (E-202)**	
Inlet pressure (kPa)	202.6500	Area (m^2)	0.2414
Outlet pressure (kPa)	405.3000	Inlet temperature (ºC)	108.3278
Power (kW)	109.5742	Outlet temperature (ºC)	100.0000
		Utility	Water
Cost		**Cost**	
Annualized capital cost ($MM/year)	0.0316	Annualized capital cost ($MM/year)	0.0376
Electricity cost ($MM/year)	0.0526	Utility cost ($MM/year)	0.0001
Compressor (K-204)		**Heater (E-203)**	
Inlet pressure (kPa)	405.3000	Area (m^2)	1.9266
Outlet pressure (kPa)	810.6000	Inlet temperature (ºC)	181.4258
Power (kW)	130.5789	Outlet temperature (ºC)	225.0000
		Utility	HP steam
Cost		**Cost**	
Annualized capital cost ($MM/year)	0.0372	Annualized capital cost ($MM/year)	0.0180
Electricity cost ($MM/year)	0.0627	Utility cost ($MM/year)	0.0383
Reactor (R-201)		**Reactor (R-202)**	
Type	PFR	**Type**	CSTR
Diameter (m)	0.1330	Volume (m^3)	5
Length (m)	2.0000	Utility	Water
Number of tubes	36.0000	Energy (kW)	379.7062
Utility	Water		
Energy (kW)	2664.0722		
Cost		**Cost**	
Annualized capital cost ($MM/year)	0.0109	Annualized capital cost ($MM/year)	0.0317
Utility cost ($MM/year)	0.0272	Utility cost ($MM/year)	0.0039
Cooler (E-205)		**Vessel (V-200)**	
Area (m^2)	5.2845	**Type**	3-phase separator
Inlet temperature (ºC)	225.0000		
Outlet temperature (ºC)	40.0000	Inlet temperature (ºC)	40.0000
Utility	Water	Pressure (kPa)	810.6000
Cost		Vapor phase	0.4630
Annualized capital cost ($MM/year)	0.0156	Molar flow (kg/h)	7304.4781
Utility cost ($MM/year)	0.0527		

Table 4. Main characteristics of equipment selected in the oxychlorination system (continued).

Column (T-200)			
Condenser (E-206)		**Reboiler (E-207)**	
Area (m^2)	2.7728	Area (m^2)	0.9944
Temperature distillate (ºC)	-53.2189	Temperature distillate (ºC)	79.0712
Utility	Refrigerant	Utility	LP steam
Cost		**Cost**	
Annualized capital cost ($MM/year)	0.0331	Annualized capital cost ($MM/year)	0.0685
Utility cost ($MM/year)	0.1078	Utility cost ($MM/year)	0.0952
Trays and tower			
Material of construction	Carbon steel	Number of trays [N_t]	10.0000
Tray spacing (m)	$H_t = 0.6096$	Diameter (m)	0.5246
Column height (m)	$H = 3 + N_t \cdot H_t$	Annualized capital cost ($MM/year)	0.0067
Column (T-201)			
Condenser (E-208)		**Reboiler (E-209)**	
Area (m^2)	41.5572	Area (m^2)	24.1020
Temperature distillate (ºC)	62.7384	Temperature distillate (ºC)	113.5267
Utility	Water	Utility	LP steam
Cost		**Cost**	
Annualized capital cost ($MM/year)	0.0196	Annualized capital cost ($MM/year)	0.0185
Utility cost ($MM/year)	0.0093	Utility cost ($MM/year)	0.3717
Trays and tower			
Material of construction	Carbon steel	Number of trays [N_t]	20.0000
Tray spacing (m)	$H_t = 0.6096$	Diameter (m)	0.8484
Column height (m)	$H = 3 + N_t \cdot H_t$	Annualized capital cost ($MM/year)	0.0153

Table 5. Main characteristics of equipment selected in the pyrolysis system.

Heater (E-300)			
Area (m^2)	5.7292	**Cost**	
Inlet temperature (ºC)	83.4251	Annualized capital cost ($MM/year)	0.0155
Outlet temperature (ºC)	200.0000	Utility cost ($MM/year)	0.2427
Utility	HP steam		
Compression system			
Type	Three-stage compression		
Compressor (K-303)		**Cooler (E-302)**	
Inlet pressure (kPa)	101.3250	Area (m^2)	1.3905
Outlet pressure (kPa)	405.3000	Inlet temperature (ºC)	251.7792
Power (kW)	687.6363	Outlet temperature (ºC)	200.000
		Utility	Water
Cost		**Cost**	
Annualized capital cost ($MM/year)	0.1531	Annualized capital cost ($MM/year)	0.0193
Electricity cost ($MM/year)	0.3301	Utility cost ($MM/year)	0.0022
Compressor (K-304)		**Cooler (E-303)**	
Inlet pressure (kPa)	405.3000	Area (m^2)	2.4722
Outlet pressure (kPa)	810.6000	Inlet temperature (ºC)	303.2558
Power (kW)	421.7447	Outlet temperature (ºC)	200.0000
		Utility	Water
Cost		**Cost**	
Annualized capital cost ($MM/year)	0.1036	Annualized capital cost ($MM/year)	0.0171
Electricity cost ($MM/year)	0.2024	Utility cost ($MM/year)	0.0043
Compressor (K-305)		**Heater (E-304)**	
Inlet pressure (kPa)	810.6000	Area (m^2)	4.3766
Outlet pressure (kPa)	2063.4038	Inlet temperature (ºC)	343.0175
Power (kW)	584.1500	Outlet temperature (ºC)	471.4226
		Utility	Fuel oil
Cost		**Cost**	
Annualized capital cost ($MM/year)	0.1347	Annualized capital cost ($MM/year)	0.0165
Electricity cost ($MM/year)	0.2804	Utility cost ($MM/year)	0.2145
Reactor (R-300)		**Cooler (E-306)**	
Type	PFR	**Type**	Cooler
Diameter (m)	0.6180	Area (m^2)	14.7338
Length (m)	20.0000	Inlet temperature (ºC)	471.4226
Number of tubes	50.0000	Outlet temperature (ºC)	32.2022
Utility	Fuel oil	Utility	Water
Energy (kW)	1499.6086		
Cost		**Cost**	
Annualized capital cost ($MM/year)	0.1024	Annualized capital cost ($MM/year)	0.0163
Utility cost ($MM/year)	0.6133	Utility cost ($MM/year)	0.2289
Pump (P-300)			
Adiabatic efficiency (%)	75.0000	**Cost**	
Inlet pressure (kPa)	2063.4038	Annualized capital cost ($MM/year)	0.0029
Outlet pressure (kPa)	2335.0097	Utility cost ($MM/year)	0.0007
Power (kW)	1.3842		

Table 5. Main characteristics of equipment selected in the pyrolysis system (continued).

Column (T-300)			
Condenser (E-307)		**Trays and tower**	
Temperature distillate (ºC)	26.7931	Material of construction	Carbon steel
Utility	Water	Number of trays [N_t]	15.000
Cost		Tray spacing (m)	$H_t = 0.6096$
Annualized capital cost ($MM/year)	0.4420	Column height (m)	$H = 3 + N_t \cdot H_t$
Utility cost ($MM/year)	0.0003	Diameter (m)	0.3487
		Annualized capital cost ($MM/year)	0.0176
Column (T-301)			
Condenser (E-308)		**Reboiler (E-309)**	
Temperature distillate (ºC)	0.7869	Temperature distillate (ºC)	231.6219
Utility	Refrigerant	Utility	HP steam
Cost		**Cost**	
Annualized capital cost ($MM/year)	0.0202	Annualized capital cost ($MM/year)	0.0223
Utility cost ($MM/year)	0.0672	Utility cost ($MM/year)	0.4726
Trays and tower			
Material of construction	Carbon steel	Number of trays [N_t]	39.0000
Tray spacing (m)	$H_t = 0.6096$	Diameter (m)	0.5577
Column height (m)	$H = 3 + N_t \cdot H_t$	Annualized capital cost ($MM/year)	0.0633

Table 6. Mass flows and prices of products and raw materials.

	Mass flow (kg/h)	Utility cost ($MM/year)
Raw material		
Ethylene	2083.4214	20.6234
Cl_2	4077.4712	8.1281
HCl	0.4238	0.0003
O_2	892.2568	0.2867
Product		
TCE	2657.0717	26.9959
VCM	4652.0717	24.4880

Table 7. Steams involved in the heat integration.

	T_{in} (ºC)	T_{out} (ºC)	$F \cdot C_p$ (kW/ºC)	Type
H1	73.0941	72.0941	2673.6591	Hot
H2	73.0941	40.0000	2.0826	Hot
H3	-26.8069	-27.8069	39.6429	Hot
H4	45.6500	40.0000	1.6529	Hot
H5	108.3278	100.0000	1.7091	Hot
H6	225.0000	224.0000	2664.0722	Hot
H7	225.0000	224.0000	379.7062	Hot
H8	225.0000	40.0000	2.3749	Hot
H9	-53.2189	-54.2189	103.7722	Hot
H10	62.7384	61.7384	912.1067	Hot
H11	251.7792	200.0000	4.2631	Hot
H12	303.2558	200.0000	4.1830	Hot
H13	471.4226	32.2022	5.8558	Hot
H14	26.7931	25.7931	2.4989	Hot
H15	0.7869	-0.2131	295.5232	Hot
C1	22.7518	73.0941	1.3371	Cold
C2	82.6478	83.6478	1.1352	Cold
C3	181.4258	225.0000	1.8075	Cold
C4	79.0712	80.0712	65.9928	Cold
C5	113.5267	114.5267	918.4802	Cold
C6	83.4251	200.0000	4.0908	Cold
C7	343.0175	471.4226	4.7299	Cold
C8	471.4226	472.4226	1499.6086	Cold
C9	231.6219	232.6219	927.0966	Cold

Table 8. Utility needed on the VCM plant.

	Economically optimized plant	**Heat integrated plant**
Heating requirements (kW)		
LP steam	1162.8131	0.0000
HP steam	1478.2870	0.0000
Fuel oil	2024.0745	1546.908
Cooling requirements (kW)		
Water	7794.7779	7254.3630
Refrigerated water 5 ºC	2280.2925	38.4697
Refrigerant low temperature -20 ºC	295.5232	295.5232
Refrigerant very low temperature -50 ºC	18.9159	39.6429
Refrigerant extremely low temperature -100 ºC	103.7722	103.7722
Utility cost (MM$/year)	2.5713	0.8683

Table 9. Data prices for raw materials, products, and utilities.

Raw material / Product	**Price range ($/kg)**	**Utility**	**Price range ($/kWh)**
Ethylene	0.9813 – 1.4934	Cooling water	0.0013
Cl_2	0.1839 – 0.3145	Refrigerated water	0.0159
HCl	0.0744 – 0.0909	Low temperature refrigerant	0.0284
		Very low temperature refrigerant	0.0472
VCM	0.6827 – 0.7680	Extremely low temperature refrigerant	0.0900
TCE	1.1094 – 1.1947	LP steam	0.0506
		HP steam	0.0637
		Fuel oil	0.0460 – 0.0562
		Electricity	0.0540 – 0.0660

Table 10. Triangular probability distribution model parameters.

	Ethylene ($/kg)	**Cl_2 ($/kg)**	**HCl ($/kg)**	**VCM ($/kg)**	**TCE ($/kg)**	**Electricity ($/kWh)**	**Fuel oil ($/kWh)**
a	0.8832	0.1655	0.0670	0.6144	0.9984	0.0486	0.0414
b	1.6427	0.3459	0.1000	0.8448	1.3142	0.0726	0.0618
c	1.2374	0.2492	0.0827	0.7253	1.1520	0.0600	0.0511

Table 11. Expected value, variance, and standard deviation of the raw material and product prices.

	Ethylene ($/kg)	**Cl_2 ($/kg)**	**HCl ($/kg)**	**VCM ($/kg)**	**TCE ($/kg)**	**Electricity ($/kWh)**	**Fuel oil ($/kWh)**
Expected value *E[X]*	1.2544	0.2535	0.0832	0.7282	1.1549	0.0604	0.0514
Variance *Var[X]*	0.0241	0.0014	0.0000	0.0022	0.0042	0.0000	0.0000
Standard deviation *sd[X]*	0.1551	0.0369	0.0068	0.0470	0.0645	0.0049	0.0042